Multichannel SAR Imaging using Wavefront Reconstruction

Luke Rosenberg[1-3] **Doug Gray**[1-2]

[1] Electrical Engineering Department, University of Adelaide
North Terrace, Adelaide SA, Australia 5005
email: luker@eleceng.adelaide.edu.au
email: dgray@eleceng.adelaide.edu.au
[2] Cooperative Research Center for Sensor, Signal and Information Processing (CSSIP)
[3] Defence, Science and Technology Organisation (DSTO)

Abstract: The combination of phased arrays with Synthetic Aperture Radar (SAR), ie. multichannel SAR offers many benefits such as improved ambiguity suppression for Moving Target Indication (MTI) and imaging large swaths [1]-[2], improved Signal-Noise-Ratio (SNR) [3] and the potential to suppress spatial jammers by use of Space Time Adaptive Processing (STAP) [4].

Classical SAR imaging is based on analogue/optical techniques and includes polar format and range-doppler based imaging. More precise imaging algorithms are based on wavefront reconstruction [5], and offer the potential for imaging with greater accuracy. Soumekh [6], has summarised a number of these including spatial MF interpolation, range stacking and time domain correlation. While multichannel SAR imaging has been addressed by [4], there has been no comprehensive study on how different wavefront reconstruction algorithms can be implemented for focussing multichannel data. This work extends these three SAR wavefront reconstruction algorithms to include multiple transmit and receive antennas and provides a quantitative comparison of their Point Spread Functions (PSF).

1. Introduction

Existing work in multichannel SAR imaging has covered Matched Filter (MF) processing [4], orthogonal reference vectors for MTI [2] and sidelobe suppression vectors for long-range low pulse repetition frequency or non-ideal antenna patterns [2] [7]. MF processing is concerned with obtaining optimal SNR contributions for each pixel and may contain sidelobe leakage from neighbouring pixels. Orthogonal reference vectors are used to prevent sidelobe leakage and are essentially an MTI technique to form an image without contributions from stationary scatterers. Sidelobe suppression vectors act as a compromise between the two, reducing sidelobe leakage by minimising the total output power of the filter while ensuring enough energy is obtained from the desired pixel. For most cases of SAR imaging, the sidelobe leakage between pixels is low enough that MF processing is acceptable and this paper is primarily concerned with algorithms using this method.

The three imaging algorithms investigated are based on the MF solution to Green's function [8], which describes how the measured data can be used to represent real world imaging coordinates. Throughout this paper, each array element transmits and receives and range processing has been performed prior to imaging.

2. Imaging Introduction

Consider a SAR travelling along the y-axis, imaging a patch in the slant-plane $x \in [-X_0, X_0]$, $y \in [-Y_0, Y_0]$, where the received data from each channel is base-banded and range processed to remove the effect of range compression. The signal from the n^{th} array element S_n is now defined in the (ω, u) domain, where ω is the fast-time frequency and u represents the SAR platform position,

$$S_n(\omega, u, x, y) = \exp\left[-2jkR(x + X_c, y - u - 0.5d_n)\right], \tag{1}$$

The radial distance $R(x, y) = \sqrt{x^2 + y^2}$, the wavenumber, $k = \omega/c$, the antenna locations $d_n = (n - 1)\delta$, for antenna spacing δ and to keep the phase center at center of the array, $n \in [-(N-1)/2, (N-1)/2]$ for N (odd) antenna elements. The signal can then be stacked for each channel to give the signal vector

$$\mathbf{S}(\omega, u, x, y) = [S_{-(N-1)/2}(\cdot), \ldots, S_{(N-1)/2}(\cdot)]^T. \tag{2}$$

The imaging model in the (ω, u) domain is given by

$$\mathbf{X}(\omega, u) = \int_y \int_x f(x, y)\mathbf{S}(\omega, u, x, y)dxdy \tag{3}$$

where $f(x, y)$ is the reflectivity of the patch being imaged. It can be shown using [6] with a slight extension to include multiple channels, that the inverse of this equation is given by

$$f(x, y) = \int_{k_u} \int_{\omega} \mathbf{S}^H(\omega, k_u, x, y)\mathbf{X}(\omega, k_u)d\omega dk_u, \tag{4}$$

where both $\mathbf{X}(\omega, u)$ and $\mathbf{S}(\omega, u, x, y)$ have been Fourier Transformed into the slow-time frequency domain (k_u) and the slowly fluctuating amplitude terms have not been included. The form of the signal model in this equation is given by,

$$S_n(\omega, k_u, x, y) = \exp\left[-j\sqrt{4k^2 - k_u^2}(x + X_c) - jk_u(y - 0.5d_n)\right]. \tag{5}$$

The multichannel MF imaging equation 4 forms the basis for the three wavefront imaging algorithms:

Spatial MF Interpolation The first algorithm uses a single frequency domain MF at a fixed range and performs range migration compensation by a Stolt interpolation to map from the measured to the image domain.

Range Stacking For better accuracy at the expense of extra computations, range stacking can be used. It utilises a different MF for each range and can determine the point spread function more precisely.

Time Domain Correlation Since both of the frequency domain algorithms utilise the principle of stationary phase in formulating the MF, the time domain must be used if more precise imaging is desired. Time domain correlation is the most computationally intensive of these three algorithms as the reference vector is determined precisely for each pixel.

3. Spatial Matched Filter Interpolation

Soumkeh [6], has presented this algorithm as spatial frequency interpolation for a single channel SAR. It has also been proposed for multichannel SAR by Ender [4], though his implementation is in the (ω, u) domain so it can be extended to STAP. He has also shown how this can be derived in the (ω, k_u) domain for a single range. It is this (ω, k_u) domain approach using spatial only vectors combined with the multiple range interpolation of [6] that is presented below.

The spatial MF solves the imaging equation 4 by varying ω and k_u with a fixed focus position $(0, 0)$. To implement this algorithm for multichannel SAR, a reference vector is chosen, $\mathbf{S_{ref}}(\omega, k_u) = \mathbf{S}(\omega, k_u, 0, 0)$ and hence the image in the (ω, k_u) domain can be determined by the following inner product.

$$F(\omega, k_u) = \mathbf{S}^H_{\mathbf{ref}}(\omega, k_u)\mathbf{X}(\omega, k_u) \tag{6}$$

The measurement data however, is obtained in the (t, u) domain, or once Fourier Transformed transformed, the (ω, k_u) domain. While the sampled data is evenly spaced, once transformed into the spatial frequency (k_x, k_y) domain, becomes non-evenly spaced. To form an estimate of the target reflectivity function, $f(x, y)$, range migration compensation is required and is implemented using a using Stolt Interpolation with a sinc function smoothed with a hamming window in the (k_x, k_y) domain. A block diagram summarising this algorithm is presented in Figure 1.

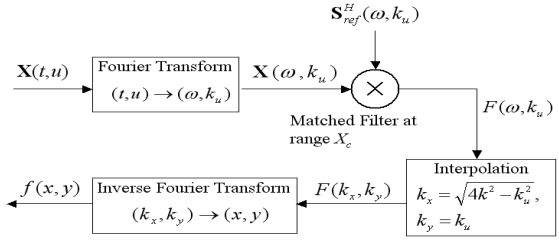

Figure 1: Spatial Matched Filter Interpolation Block Diagram

4. Range Stacking

A more exact frequency domain implementation of equation 4 is referred to as range stacking [6]. This algorithm uses a different MF reference for each of the L range bins, then numerically integrates over the fast-time frequency ω, before inverse Fourier Transforming to get the final result. By explicitly performing these steps, the interpolation step from the previous algorithm is not required and the final image does not suffer from the truncation and DFT wrap-around errors in the k_x domain. The tradeoff for this approach however is the complexity and timeliness of the algorithm.

To extend this algorithm to multichannel SAR, the reference signal for each range x_l, $l = 1 \ldots L$, can be derived from equation 5,

$$S_n(\omega, k_u, x_l, y) = \underbrace{S_n(\omega, k_u, x_l, 0)}_{S_{ref,n}(\omega, k_u, x_l)} \exp[-jk_u y] \tag{7}$$

These signals are then stacked as in equation 2 to give $\mathbf{S_{ref}}(\omega, k_u, x_l)$ and used in the range stacking imaging equation,

$$f(x_l, y) = \int_{k_u} \left[\int_{\omega} \mathbf{S}^H_{\mathbf{ref}}(\omega, k_u, x_l)\mathbf{X}(\omega, k_u) d\omega \right] \exp[jk_u y] dk_u \tag{8}$$

which must be repeated for each range bin. Figure 2 represents this algorithm in a block diagram.

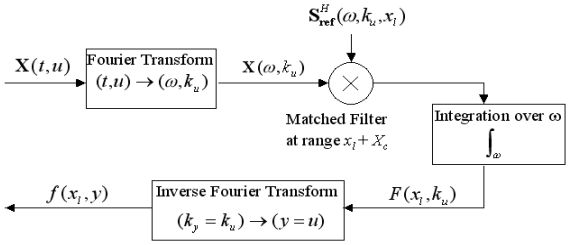

Figure 2: Range Stacking Block Diagram

5. Time Domain Correlation

SAR imaging may also be performed by convolving the SAR signal with a shift-varying filter in the time domain and this is the principle behind the Time Domain Correlation (TDC) algorithm presented by Soumekh [6]. In TDC, the processor correlates the measured SAR signal with a reference vector at a given point (x_l, y_m). This implies that the reference vector in the (t, u) domain must be calculated with a delay determined for each point. The integration is then performed over both variables to obtain the return for that point. This formulation results in the most computationally intensive of these three algorithms, but also provides also the most accurate result. To extend this algorithm for multichannel SAR, the reference vector must also include the delay to the respective antenna element.

$$s_n(t,u,x_l,y_m) = \exp\left[-j2k_c\sqrt{(x_l+X_c)^2+(y_m-u-0.5d_n)^2}\right]p(t) \tag{9}$$

where $p(t)$ is the impulse response function after range processing. After stacking the reference vector via equation 2 to give $\mathbf{s_{ref}}(t,u,x_l,y_m)$, the imaging equation can be written in either the (t, u) domain or by using Parseval's theorem, in the (ω, u) domain as

$$\begin{aligned} f(x_l,y_m) &= \int_u\int_t \mathbf{s}_{\mathbf{ref}}^{H}(-t,u,x_l,y_m)\mathbf{x}(t,u)dtdu \\ &= \int_u\int_\omega \mathbf{S}_{\mathbf{ref}}^{H}(\omega,u,x_l,y_m)\mathbf{X}(\omega,u)d\omega du \end{aligned} \tag{10}$$

Figure 3 represents this algorithm in a block diagram.

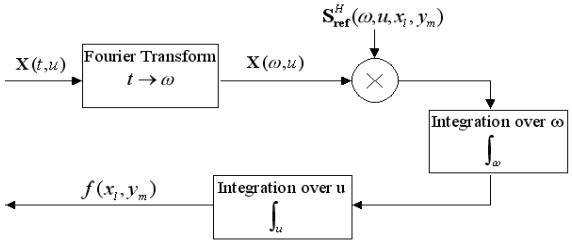

Figure 3: Time Domain Correlation Block Diagram

6. Comparative Results

These three algorithms are now tested by simulation with the parameters in Table 1:

Table 1: Simulation Parameters

Parameters	Value
Carrier Frequency / Bandwidth	10 / 0.3 GHz
Number of Elements / Spacing	5 / $\frac{\lambda_c}{2}$ m
PRI / SAR Platform Speed	1 ms / 98 ms^{-1}
Range Res. / No. Range bins	1 m / 128

SAR Run	Range Center	Azimuth Resolution	No. Pulses
1	40 m	0.2 m	128
2	4 m	0.16 m	68

The first SAR run uses a larger center range to simulate a far-field scenario, while the second run uses a smaller center range for a near-field scenario. The point spread functions (PSF) for these two cases are shown in Figures 4 and 5:

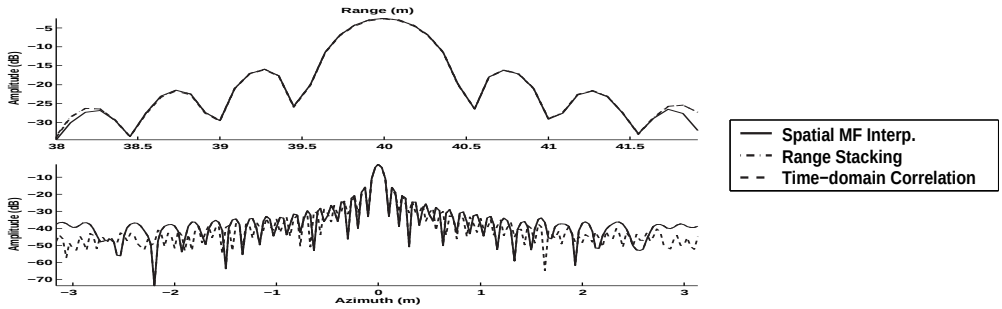

Figure 4: PSF for SAR Run 1 (Large Center Range)

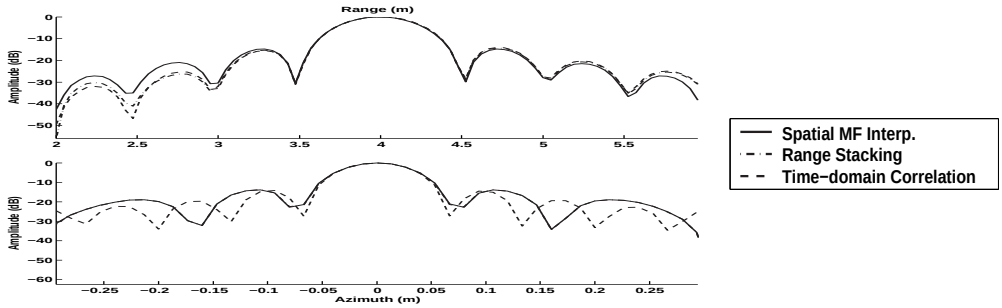

Figure 5: PSF for SAR Run 2 (Small Center Range)

For the first run, there is very little difference between the spatial MF interpolation and range stacking algorithms. This is due to the denser (k_x, k_y) sampling grid that is used in the Stolt interpolation. The time domain correlation algorithm also produces a similar range response, but on average has lower sidelobes in azimuth.

When the center range is reduced and the (k_x, k_y) sampling grid is sparser, the spatial MF interpolation algorithm produces a PSF range slice with different sidelobes. This is due to the interpolation

step which uses a sinc function smoothed with a hamming window. For the azimuth slice, the spatial MF interpolation and range stacking algorithms produce near identical results, while the time domain correlation is significantly different.

To further quantify the difference between the PSFs, the Peak Sidelobe Ratio (PSR) and the integrated Sidelobe Ratio (ISLR) can be used to determine the difference between the main-lobe and greatest side-lobe and the ratio of all energy in the sidelobes to the energy in the mainlobe. Only the azimuth slice was analysed as it produced the greatest difference between algorithms.

Table 2: Peak Sidelobe Ratio and Integrated Sidelobe Ratio Comparisons

		Spatial MF-Interp	Range Stacking	Time Domain Corr.
Run 1 (Far-field) :	PSR (dB)	13.47	13.42	13.56
	ISLR (dB)	-9.75	-9.72	-10.47
Run 2 (Near-field) :	PSR (dB)	13.87	13.81	14.15
	ISLR (dB)	-10.76	-10.61	-11.91

7. Conclusion

The results indicate that with a far-field scenario, which is the typical operating condition for SAR, the best results are achieved with the time domain correlation algorithm, while the spatial MF interpolation and range stacking algorithms offer good performance but with a higher ISLR. At near-field, the range PSF shows a minor difference between the algorithms, while the time domain correlation algorithm produces slightly better PSR and ISLR results for the azimuth PSF.

8. References

[1] N.A. Goodman, Sih-Chung-Lin, D. Rajakrishna, and J.M. Stiles. Processing of multiple-receiver spaceborne arrays for wide-area SAR. In *IEEE transactions on Geoscience and Remote Sensing, IGARSS*, volume 40, no. 4, pages 841 –852, 2002.

[2] J.H.G. Ender. Linear and non-linear techniques for multi-channel SAR image generation. In *EUSAR 2000*, 2000.

[3] M. Younis, C. Fischer, and W. Wiesbeck. Digital beamforming in SAR systems. In *IEEE transactions on Geoscience and Remote Sensing Symposium, IGARSS*, volume 41, no. 7, pages 1735 –1739, 2003.

[4] J. H. G. Ender. Space-Time Adaptive Processing for Synthetic Aperture Radar. In *IEE Colloquium on Space-Time Adaptive Processing*, 1998.

[5] J. Goodman. *Introduction to Fourier Optics*. McGraw-Hill, 1968.

[6] M. Soumekh. *Synthetic Aperture Radar Signal Processing with MATLAB Algorithms*. John Wiley & Sons, Inc., 1999.

[7] N. Goodman, D. Rajakrishna, and J. Stiles. Wide swath, high resolution SAR using multiple receive apertures. In *IEEE transactions on Geoscience and Remote Sensing Symposium, IGARSS*, volume 3, pages 1767 –1769, 1999.

[8] P. Morse and H. Feshbach. *Methods of Theoretical Physics*. McGraw-Hill, 1953.